Journal of the Optical Society of America B
OPTICAL PHYSICS

Laser cooling without spontaneous emission using the bichromatic force

CHRISTOPHER CORDER, BRIAN ARNOLD, XIANG HUA, AND HAROLD METCALF*

Physics and Astronomy, Stony Brook University, Stony Brook, New York 11794-3800, USA
**Corresponding author: harold.metcalf@stonybrook.edu*

Received 15 January 2015; revised 2 March 2015; accepted 31 March 2015; posted 31 March 2015 (Doc. ID 232627); published 21 April 2015

It is widely believed that spontaneous emission (SE) is necessary to remove entropy from an atomic sample during laser cooling. In fact, SE is needed for energy removal when laser cooling is done with single-frequency light, but with more than one frequency, both energy and entropy can be removed using only stimulated processes. Our experimental demonstration of this phenomenon works by restricting the atom–light interaction to a time short compared to a cycle of absorption followed by natural decay [Phys. Rev. Lett. 114, 043002 (2015)]. We present here additional information on these results, in particular, simulations of the motion of atoms under the bichromatic force that compare well with our data. This accomplishment is of interest to direct laser cooling of molecules or in experiments where working space or time is limited.

OCIS codes: (020.3320) Laser cooling; (020.1335) Atom optics; (140.3320) Laser cooling.

http://dx.doi.org/10.1364/JOSAB.32.000B75

1. INTRODUCTION

This paper expands upon the ideas of laser cooling without spontaneous emission (SE) presented in Refs. [1,2] by describing some of our numerical simulations that corroborate the cooling data. Reference [2] described our experiments on laser cooling in a time short compared to the cycle of absorption followed by SE. Here we provide additional experimental description and details, as well as a discussion of our simulations of the cooling process.

The use of electromagnetic radiation to exert forces on neutral atoms was first demonstrated by Frisch in 1933 [3]. The advent of stable tunable lasers has resulted in dramatic advances since that early time, and this OSA journal provided extensive reviews of the emerging field of laser cooling with two special issues in 1985 and 1989 [4,5]. There have been very many special topical conferences, review articles, and books on laser cooling that now constitute a large part of atomic physics.

The early views of the forces that produce laser cooling were dominated by the notion of two-level atoms moving in a monochromatic laser field. The momentum exchange required for the resulting radiative force proceeds by absorption followed by SE that returns atoms to their ground states for the next absorption cycle. In ordinary Doppler cooling, the SE associated with this process provides the dissipation necessary for cooling. This radiative force saturates at a maximum value of $F_{\mathrm{rad}} \equiv \hbar k\gamma/2$, where $\lambda \equiv 2\pi/k$ is the wavelength of the optical transition, and $\gamma \equiv 1/\tau$ is the excited state decay rate.

Atoms can also be returned to their ground states by stimulated emission. If this is caused by a light beam of wave vector $\vec{k}_2$ different from that of the exciting light $\vec{k}_1$, there is a momentum exchange of $\hbar(\vec{k}_1 - \vec{k}_2)$. These stimulated processes repeat at the Rabi frequency Ω that can be $\gg\gamma$. Because excited atoms then return to their ground states more frequently by stimulated emission than SE, this dipole force does not saturate at a momentum exchange rate limited by γ.

Laser cooling has been demonstrated with monochromatic light using both radiative and dipole forces [6–9]. The topics that could be described with this two-level atom model include atomic beam slowing and cooling, optical molasses, optical dipole traps, lattices and band structure effects, and a host of others [9].

A few years after the early experiments it became clear that this simple view was inadequate, and that the multiple level structure of real atoms was necessary to explain some experiments. Perhaps the most dramatic impact came from the discovery of cooling below the Doppler temperature $T_D \equiv \hbar\gamma/2k_B$ [10], where k_B is Boltzmann's constant. This could be explained only by polarization gradient cooling in atoms with multiple ground state levels, and was labeled "Sisyphus cooling" by the authors of Ref. [11]. In such sub-Doppler cooling of multilevel atoms, it is typically the dipole force that works on the atoms.

As discussed in Ref. [2], these single-frequency cooling techniques necessitate that the outgoing light from SE is the only way to remove thermal (kinetic) energy from the atoms. This is required because all stimulated light from applied monochromatic laser fields must occur at the same frequency, preventing any energy exchange between the light and atoms. Only SE

combined with the Doppler shift resulting from atomic motion can remove more energy than was absorbed in the excitation, thereby allowing the energy exchange required for cooling. For example, single-frequency cooling works in Doppler molasses because the cooling laser light at ω_ℓ is always tuned below the atomic resonance frequency ω_a by $\delta \equiv \omega_\ell - \omega_a$. In sub-Doppler laser cooling schemes such as Sisyphus cooling (polarization gradient), the fluorescence has a higher frequency than the absorbed light by approximately the difference of the ground state sublevels' light shifts, thereby dissipating energy.

When the early view of laser cooling consisting of two-level atoms moving in monochromatic fields was replaced by a more complete description of the multilevel structure of atoms, many more phenomena could be described. In addition to the Sisyphus cooling discussed above, there is the magneto-optic trap (multiple excited state levels) and velocity selective coherent population trapping (multiple ground state levels). Thus the extension from two-level to multilevel atoms gave an unexpected richness to the topic of atomic motion in optical fields. It seems natural to expect that a comparable multitude of new phenomena is to be found for the motion of atoms in multi-frequency fields, but this subject, discussed next, has not received as much attention.

2. OPTICAL FORCES IN POLYCHROMATIC LIGHT

One of the primary advantages of polychromatic light for exerting optical forces on atoms and cooling them is the huge magnitude of such forces. The strength of the force arises from the use of stimulated emission in place of SE to return atoms to their ground states, and this enables rapid, repeated momentum exchanges with the light field. The rate of momentum exchange and the velocity range of these forces are not limited by the properties of the atoms being cooled. Instead, these characteristics can be chosen by the experimenter through the laser parameters when implemented by either the bichromatic force [12–14] or adiabatic rapid passage [15–17]. In addition, in a polychromatic light field, energy can be removed by purely stimulated processes if absorption of the lower frequency light (i.e., red) is followed by stimulated emission into the higher frequency (blue) field.

A. Dipole Force Rectification

Although the nonsaturable dipole force is a very attractive tool for manipulating atoms, its practical utility is limited because its sign alternates on the wavelength scale so its spatial average vanishes. The desire to extend its spatial range has produced two related proposals that exploited two-frequency fields to provide spatial rectification of the dipole force [18,19]. Apart from the use of multiple frequencies to compensate optical pumping effects in multilevel atoms, these were the first applications of two-frequency light to optical forces.

One of these methods, rectification of the dipole force, uses two standing waves of different frequencies, with one of them intense enough to provide a strong dipole force [20]. Then the light shift from the other one with very different parameters can be used to spatially modulate the atomic transition frequency ω_a. This modulation reverses the sign of the light shift caused by the beam at the first frequency with approximately the same spatial period as the force, and therefore the force is rectified. This scheme was subsequently demonstrated [20–23]. However, the frequencies have to be fairly well specified, and therefore the rectification mechanism can tolerate only small Doppler shifts, putting rather severe limits on the velocity range of this rectified force.

B. Bichromatic Force

1. Eigenvalues in Two-Frequency Light

A second way to extend the spatial range of the dipole force uses an optical field having two beams of equal intensities and large detunings (relative to γ) that provide both a force much stronger than F_{rad} and a velocity range much wider than $\pm\gamma/k$ of the radiative force [12]. This bichromatic force arises from the coherent control of the momentum exchange between the atom and the laser fields associated with a long sequence of rapid absorption–stimulated emission cycles.

The bichromatic force is implemented with two overlapped standing waves equally detuned from atomic resonance by $\pm\delta$ with $|\delta| \gg \gamma$. Its magnitude, F_B, depends on the choice of δ, the Rabi frequency Ω, and the spatial phase offset of the standing waves. It is weakly velocity dependent over a wide velocity range $\pm\Delta v_B \approx \pm\delta/2k$ that is $\gg\gamma/k$ [12,14]. It has been demonstrated in Na [21], Cs [12], Rb [24,25], and He [13,26].

The bichromatic force is best understood using a modified dressed atom picture that was first presented in Ref. [27] and extended in Ref. [14]. The dressed atom picture is expanded to include the two laser fields at frequencies $\omega_{r,b}$. This results in a quasi-infinite manifold of discrete energy states separated by $\hbar\delta$, as shown in Fig. 1. The strength of each of these fields is described by an appropriate Rabi frequency $\Omega_{r,b}$, and along with the atomic states $|e\rangle$ and $|g\rangle$, the basis set of the system has elements such as $|g, r, b\rangle$, as shown in Fig. 1.

Each of these basis states is connected to its two adjacent states by off-diagonal matrix elements given by the Ω's of either

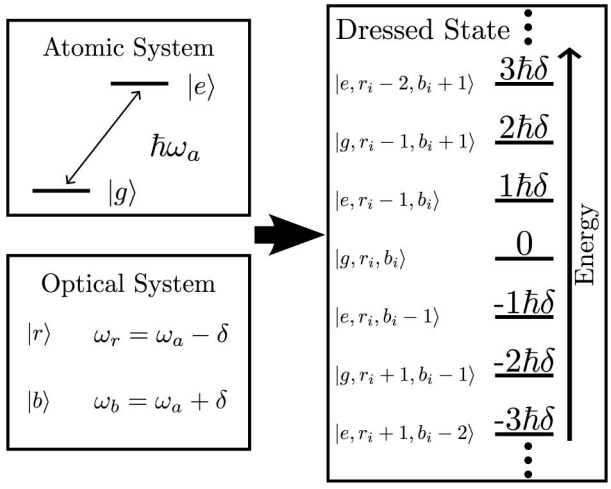

Fig. 1. Bichromatic dressed states are constructed by combining the atomic states with the energy states of the optical fields. The result is an infinite set of dressed states, each separated by $\hbar\delta$ and coupled to its neighboring states through one of the two optical frequencies.

the red or the blue detuned field, producing the Hamiltonian matrix (truncated to 7×7)

$$\mathcal{H} = \hbar \begin{bmatrix} 3\delta & \Omega_r & 0 & 0 & 0 & 0 & 0 \\ \Omega_r & 2\delta & \Omega_b & 0 & 0 & 0 & 0 \\ 0 & \Omega_b & \delta & \Omega_r & 0 & 0 & 0 \\ 0 & 0 & \Omega_r & 0 & \Omega_b & 0 & 0 \\ 0 & 0 & 0 & \Omega_b & -\delta & \Omega_r & 0 \\ 0 & 0 & 0 & 0 & \Omega_r & -2\delta & \Omega_b \\ 0 & 0 & 0 & 0 & 0 & \Omega_b & -3\delta \end{bmatrix}. \quad (1)$$

Diagonalizing this Hamiltonian matrix produces light shifts, and because the Ω's represent standing waves, the resulting eigenvalues are also spatially dependent and periodic on the scale of $\lambda/2$.

Moreover, the interference of the two standing wave fields also imposes a periodicity on the scale of $\pi c/\delta$. With $\delta \sim 10^8$ s^{-1}, this is typically a few meters and is very much larger than the millimeter scale of our experiments. We therefore consider the spatial phase offset of the standing waves as a fixed experimental parameter under our control. For a standing wave spatial offset of $\lambda/8$, these eigenvalues oscillate, as shown in Fig. 2(a) with the light field of Fig. 2(b).

As discussed above, the two-frequency system is different from the single-frequency case because it is able to add or remove energy from the atom through absorption from one frequency followed by stimulated emission into the other. This process occurs when atoms pass through the positions indicated by the small circles labeled "A" in Fig. 2(a). The energy levels undergo exact crossings because they occur between states coupled by one field at the nodal points of the other field (see vertical lines in Fig. 2).

The magnitude of the bichromatic force can be evaluated by considering the path of an atom along these energy states (as indicated by the heavy curved arrow) and is given by

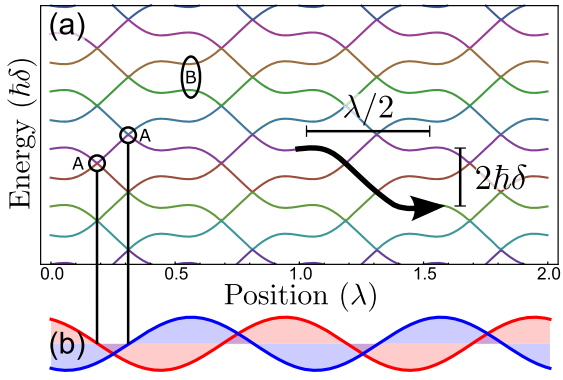

Fig. 2. Part (a) shows the eigenvalues of the two-frequency dressed state system separated by $\hbar\delta$ where the two fields have equal amplitudes and a spatial phase offset of $\lambda/8$. The curved arrow indicates a typical path followed by an atom moving to the right. Circled transition points of the type marked "A" are exact crossings because they occur at the nodes of the standing wave fields shown in part (b). For our case, this occurs for $\Omega = \sqrt{3/2}\delta$. Point "B" in the vertical ellipse marks the location of a possible Landau–Zener transition (figure from Ref. [2]).

$$F_B = -\frac{\langle \Delta E \rangle}{\Delta z} = \frac{2\hbar\delta}{\lambda/2} = \frac{2\hbar k\delta}{\pi}. \quad (2)$$

Since we typically choose $\delta \gg \gamma$ for our experiments, the force $F_B \gg F_{\text{rad}}$.

2. Velocity Dependence of the Bichromatic Force

In order to be effective, a laser cooling force must be significant over some velocity range but minuscule at other velocities. This causes a displacement of atoms from one region of velocity-space to another without significant removal of atoms from the destination region. The result is a net reduction in a region of occupied velocity-space. The velocity dependence of various cooling forces arises from different mechanisms, as discussed in Ref. [2], but it is important to emphasize here again that none of these mechanisms arises directly from SE processes.

Explaining this mechanism for the bichromatic force is straightforward. Atoms can undergo many Rabi cycles involving two transitions with the same light frequency, either red or blue, and experience momentum changes of zero or $\pm 2\hbar k$ each time. But the resulting energy change is only of the order of a few times the recoil energy $\hbar\omega_r \equiv \hbar^2 k^2/2M \ll \hbar\delta$, and is not large enough to cause a transition to an adjacent eigenstate that is $2\hbar\delta$ away. Instead, the energy change is compensated by the atomic motion in the spatially dependent potential produced by the light shifts that are $\sim\hbar\delta$ [see Fig. 2(a)].

However, when a Rabi cycle exchanges red light for blue, or vice versa, there is an energy change of $2\hbar\delta$ that must be compensated by an atomic kinetic energy change of $\Delta E_{\text{KE}} = v\Delta p$. Since Δp can be a few times $2\hbar k$ resulting from monochromatic Rabi cyles during a traversal of $\lambda/2$ [see curved arrow in Fig. 2(a)], we find $v \leq \delta/k$. More careful considerations lead to $\Delta v_B \approx \delta/2k$. Thus the bichromatic force accelerates atoms to velocities near $v = \pm\Delta v_B$, where the magnitude of the force diminishes sharply.

Atoms with velocities approaching Δv_B can follow paths along the eigenstates in Fig. 2(a) with energy change $<2\hbar\delta$ by making nonadiabatic Landau–Zener transitions between the atomic dressed states. These are most likely to occur near anticrossings of the type indicated by the vertical ellipse labeled "B" in Fig. 2(a), and the atomic velocities would then fluctuate around Δv_B. Thus the final velocity distribution will be peaked near $\pm\Delta v_B$ [28] and both F_B and Δv_B scale with the value of δ. From Eq. (2) we can define a characteristic cooling time $t_c = \pi/4\omega_r$ [2]. A Galilean coordinate transformation or a frequency offset of the light fields can bring the velocity Δv_B to zero in a chosen reference frame.

Estimation of the probability p_{NA} of a nonadiabatic transition at the avoided crossing begins with the model Hamiltonian for Landau–Zener transitions:

$$\mathcal{H}_{\text{LZ}} = \begin{bmatrix} -At & B \\ B & At \end{bmatrix}. \quad (3)$$

Here the parameters A and B serve only to describe the model energy levels in the simplest, symmetrical case of a "level crossing" produced by an external parameter, in this case t [29]. Thus plots of the energies versus t are straight lines that intersect at $t = 0$ in the absence of any coupling between them

($B = 0$), and otherwise are hyperbolae of closest approach $2B$. Then the LZ model gives

$$p_{\mathrm{NA}} = e^{-\pi B^2/\hbar A} \equiv e^{-v_{\mathrm{LZ}}/v}, \tag{4}$$

because $A = v\nabla E$ for atoms moving at uniform velocity v. A rough estimate of v_{LZ} has been discussed in Ref. [14] and can be of the order $\delta/2k$.

3. Entropy Considerations

It may seem disconcerting that cooling can proceed without SE since stimulated processes are unitary and reversible and therefore provide no dissipation mechanism. But we stress that a proper description of laser cooling requires that both the atoms *and* the light must be considered as part of a single system to provide a complete description. Moreover, the absence of a reservoir in the thermodynamic sense requires that entropy be considered differently, and here we choose the number of states accessible to the system as a proper measure. For example, in the familiar case of common laser cooling experiments up to now, the 4π solid angle of the SE provides so many states accessible to the combined system of (atoms + light) that it seems natural to assume that the entropy loss of the cooled atoms is also dissipated by this light.

However, the interpretation that SE is therefore required for entropy dissipation is misleading. A description of how the light fields can serve as entropy sinks in laser cooling has been provided in Ref. [1], where ground state atoms (pure state) interact with multiple incoming laser beams (pure states) to form a mixed state even with purely stimulated processes. The fact is that monochromatic light cannot cool atoms by stimulated processes only, but polychromatic light fields can mediate both energy and entropy exchange.

It is important to recognize that the stimulated interaction between the light and the atoms is not dissipative because it is completely reversible and is a unitary process. The light has to be considered along with the atoms as a part of the system under study [1], and therefore the light field cannot be considered as a coherent state in the presence of atoms. Atoms can absorb light out of one of the laser modes, and the state of the light field must change as a consequence. Excited atoms can undergo stimulated emission and add to the energy of the light field, resulting in something that is no longer a perfect coherent state. This is the point where atomic motional entropy can be transferred to the laser fields while both remain part of the "system" [1]. Thus the atom–light interaction is simply an exchange of energy and entropy within the "system" under study. Then the dissipation required for cooling takes place when the light carries the energy and entropy out of the system and hits the walls.

3. SIMULATIONS

We have calculated the response of the atoms in a bichromatic field for short interaction times where the traditional constant velocity approximation (dragged atom) is not valid. We numerically solve the equations of motion of the time-dependent Bloch vector $(\mathrm{u}(t), \mathrm{v}(t), \mathrm{w}(t))$ and the atomic motion $z(t)$ and $v_z(t)$. The calculation includes the SE decoherence terms to simulate our experiment accurately, but the cooling does not depend on these terms.

We begin with the interaction in terms of the complex Rabi frequency given by

$$\Omega(t) = \Omega_0 e^{-i(\omega_a t)}[e^{i(k_+ z-\delta t)} + e^{i(k_- z+\delta t)} + e^{-i(k_+ z+\delta t)} + e^{-i(k_- z-\delta t)}], \tag{5}$$

where $k_\pm \equiv k \pm \delta/c$. We use classical mechanics to calculate the positions and velocities of a set of atoms as they move through the bichromatic laser field, beginning with their various initial velocities, positions, and times. The atoms are subject to the force given by

$$F_B(z,t) = \hbar[\mathrm{u}(t)\mathrm{Re}(\nabla\Omega(t)) + \mathrm{v}(t)\mathrm{Im}(\nabla\Omega(t))]. \tag{6}$$

Since this calculation is semiclassical, it does not quantize the field or the motional states of the atoms, but it is nevertheless able to reproduce the properties expected by the dressed state model as well as the features of our data. The atomic motion can be treated classically because the atomic deBroglie wavelengths are much smaller than the optical wavelength ($Mv \gg \hbar k$). The semiclassical treatment of the field in the optical Bloch equations is equivalent to tracing over the optical states when they are included as part of the system.

The solutions give the trajectories of the Bloch vector and of the atomic motion, and we find that the velocity trajectories are the most informative as they show changes produced by the bichromatic force. We can then seek accumulations of atoms around a particular velocity to show cooling.

The atoms are initially in their ground state before entering the field so that $\mathrm{u}(0) = \mathrm{v}(0) = 0$ and $\mathrm{w}(0) = -1$. Figure 3 shows a set of velocity-space trajectories for 60 equally spaced initial velocity values between $\pm 1.25\delta/k = \pm 2.5\Delta v_B$. Each line represents a trajectory in velocity-space for a particular starting value using a Rabi frequency of $\Omega_0 = \sqrt{3/2}\delta$. The three plots show trajectories for three different relative spatial phase offsets. Models of the bichromatic force show that this phase determines the direction of the force and the same behavior is demonstrated here. This dependence is periodic with relative spatial shifts of $\lambda/2$. The acceleration diminishes sharply when the atomic velocities approach $\pm\Delta v_B = \pm\delta/2k$ and the trajectories accumulate near this velocity.

To make the effect of the cooling more clear, we run the calculation for a much larger number of equally spaced, initial velocity values and bin them in velocity and time. This is shown in Fig. 4 for 3240 initial velocity values using the same parameters as Fig. 3(c). The bin size is $\Delta v_B/17$ in velocity and 8.6 ns in time, so that each bin begins with ~1000 entries.

From both figures it is clear that within $\sim 2\pi/\delta$ (~40 ns) the velocities begin to bunch around particular values. The strong feature on the right near $\delta/2k$ (orange/red) is the expected accumulation of the cooled atoms based on the dressed state model. It begins to form very rapidly, in a time well less than our atomic lifetime, ≈106 ns. The other smaller peaks may be dependent on initial conditions.

Even though the experiment runs for a time allowing the chance of ~1 SE, the cooling is not a consequence of this. When we evaluated the simulation for the nonphysical case of no SE, the result was very similar to that shown in Fig. 4.

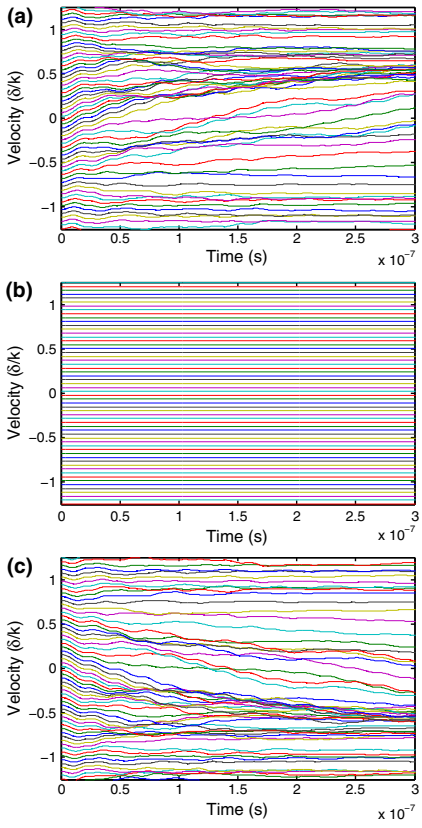

Fig. 3. Each plot shows the atomic velocity trajectories for 300 ns in the bichromatic field. The accumulation of atoms near $\pm\Delta v_B \approx \delta/2k$ is quite clearly shown, and is more pronounced when we plot these trajectories on a longer time scale. Our experiment runs for approximately 220 ns. Part (a) is for spatial phase offset $-\lambda/8$, part (b) is for phase = 0, and part (c) is for phase $+\lambda/8$.

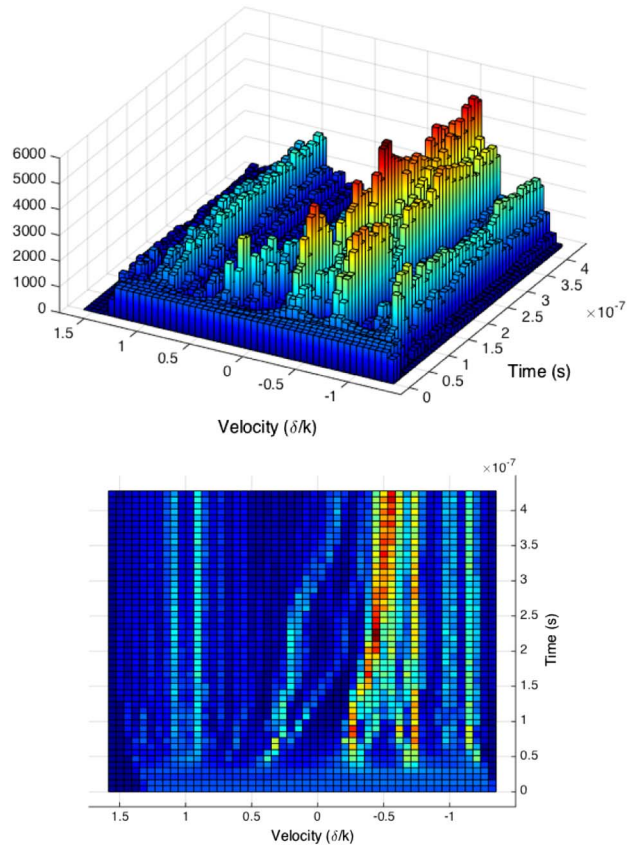

Fig. 4. Results of the simulation for 3240 equally spaced initial velocities. The local density of trajectories is counted in bins of size $\Delta v_B/17 \times 8.6$ ns. The top plot is a three-dimensional view of the density of trajectories in velocity as a function of time in a bichromatic field with a spatial phase offset of $\lambda/8$ and Rabi frequency $\sqrt{3/2}\delta$. The lower plot is of the same results, shown in two dimensions with the density designated by color in each bin.

The very short interaction time does not allow the internal atomic response to reach a steady state normally produced by SE. Consequently, the initial conditions of each atom become important and can be seen in our calculated trajectories. Even for atoms with the same initial starting velocity, entering the light field at a different location or different time can lead to a different trajectory. While all trajectories over long times converge to the same Δv_B limit, their paths can vary with these initial conditions.

The results of the simulation for velocity trajectories in a bichromatic field with spatial phase offset $\lambda/8$ and Rabi frequency $\Omega_0 = \sqrt{3/2}\delta$ are shown in Fig. 5. Figures 5(a) and 5(b) show trajectories for two different starting positions in the field separated by $\lambda/8$ (not to be confused with the spatial phase offset) with all other parameters unchanged. The overall trend for atoms within the capture range toward $-\Delta v_B$ still occurs, but the individual paths differ. Figures 5(c) and 5(d) show velocity trajectories for two runs with all parameters the same except two values of initial time separated by $\pi/4\delta$. Here the same trend exists with differing trajectories. The trajectories are invariant for shifts in starting position of $\lambda/2$ and shifts in starting time of π/δ. The invariance with spatial shifts of $\lambda/2$ is in agreement with the dressed state levels shown in Fig. 2. The π/δ time invariance agrees with the π-pulse model [12] where the traveling wave fields repeat on the time scale of a bichromatic beat.

4. EXPERIMENTAL SETUP

In Ref. [2] we described the apparatus used for our experiments. For completeness it is repeated here, albeit with the addition of Fig. 6 and several other additions and changes.

A. Laser System

Since SE cannot be eliminated, we have chosen to demonstrate bichromatic cooling using an atomic transition with a large ω_r and relatively long τ. We use the He $2^3S \rightarrow 3^3P$ transition at $\lambda = 389$ nm where $\omega_r = 2\pi \times 330$ kHz so that $t_c \approx 380$ ns. Since $\tau \approx 106$ ns and the time averaged excited state population is ~0.4 [30], the average SE time is $t_{SE} \approx 260$ ns. Thus we expect an average of <1.5 SE event during time t_c.

The $\lambda = 389$ nm light for the optical standing waves is produced by a frequency-doubled, cw, narrow linewidth Ti:sapphire laser of wavelength 778 nm [see Fig. 6(a)]. This laser is frequency locked to better than γ with a stable cavity

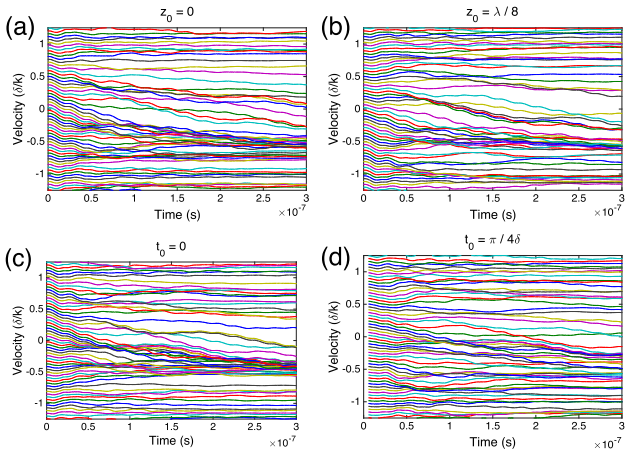

Fig. 5. Each plot shows velocity trajectories from the same bichromatic field (phase $= \lambda/8$, $\Omega = \sqrt{3/2}\delta$) but having different initial conditions. Plots (a) and (b) have the same initial starting time, but different starting positions separated by $\lambda/8$. Plots (c) and (d) start at the same position but enter the field at different initial times separated by $\pi/4\delta$.

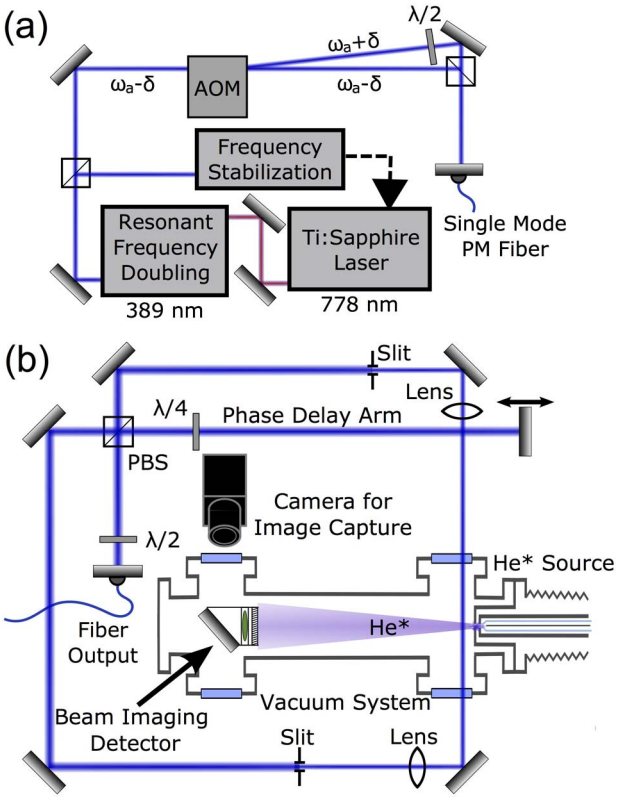

Fig. 6. Part (a) shows the uv light production by frequency doubling light from a Ti:sapphire laser. The two frequencies are produced with an acousto-optic modulator and recombined in a polarization maintaining optical fiber. Part (b) shows the exit of the bichromatic beam from the transport fiber and the optical setup at the atomic beam. The two paths are apertured with slits that are imaged onto the atomic beam to determine the interaction time. The transverse spatial distribution of the atomic beam is imaged downstream with a microchannel plate and phosphor screen to measure the bichromatic cooling.

whose length is controlled by feedback from a saturated absorption spectroscopy signal. This signal is derived from an rf discharge cell of He at $\lambda = 389$ nm, but detuned from resonance by $-\delta$ with an acousto-optic modulator (AOM).

The frequency-doubled light passes through another AOM operated at 2δ and 50% diffraction efficiency to produce two beams at $\omega_\ell = \omega_a \pm \delta$ [see Figs. 6(a) and 7(a)]. The two beams are recombined with a polarizing beamsplitter (PBS) and coupled into an ultraviolet (uv) polarization-maintaining single-mode optical fiber, suitable for both polarizations, for spatial mode matching and for transport to the vacuum system. After exiting this fiber, the two orthogonally polarized frequencies are separated by another PBS oriented at 45 deg to the orthogonal linear polarizations, resulting in two linearly polarized bichromatic beams, as shown in Fig. 6(b) [12].

The bichromatic standing waves are formed by orienting these two beams (each having both frequencies $\omega_a \pm \delta$) to be counterpropagating and aligned transverse to the He beam, as shown in Fig. 6(b). The spatial phase offset is set using a variable phase delay arm. To ensure a short interaction time, the Gaussian beams of 400 μm waists (800 μm $1/e^2$ full width) were masked by adjustable slits that were imaged directly on the atomic beam to minimize diffraction effects. The peak Rabi frequencies varied by <10% across the light field.

To ensure the desired exact crossings at the points labeled "A" in Fig. 2(a), there are two constraints. One is the total absence of coupling to other states, as discussed earlier, and the other is that the light shifts must cause the dressed state eigenvalues to just meet as shown. These conditions are connected via the relative spatial phase of the standing waves as discussed in Ref. [14]. For our choice of spatial phase offset $= \lambda/8$ [see Fig. 2(b)], the Rabi frequencies of each traveling wave component must satisfy $\Omega = \sqrt{3/2}\delta$.

We tune our laser light to the transition from the $J = 1$ ground state to the $J = 2$ excited state since tuning to the $J = 1$ or $J = 0$ excited states would preclude some of the atoms because of the selection rules. We choose linearly polarized light to excite $\Delta m_J = 0$ transitions, as shown in Fig. 7(b), because the three allowed π transitions have roughly the same strengths, with $3J$ values and hence Rabi frequencies in the ratio of $\sqrt{3}:2:\sqrt{3}$ for a fixed light intensity. Any other polarization choice would result in larger differences among the Rabi frequencies. The unpolarized atomic beam could not be optically pumped upstream of the bichromatic interaction region because of space constraints.

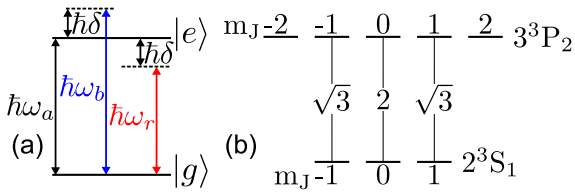

Fig. 7. Part (a) shows the two atomic levels and the detuning $\delta \gg \gamma$. Part (b) shows the $\Delta m = 0$ transitions driven by the linearly polarized light between the $J = 1$ and $J = 2$ He levels and their relative Rabi frequencies (figure from Ref. [2]).

B. Atomic Beam

Our experiment was performed on a beam of He atoms initially excited to the 2^3S state by a continuous flow, dc-discharge source, cooled with liquid N_2 to produce an average longitudinal beam velocity of ~1050 m/s [31,32]. Our one-dimensional cooling axis is oriented perpendicular to the axis of this diverging atomic beam, as shown in Fig. 6(b), and narrows its transverse velocity distribution, thereby producing partial collimation.

The atomic beam emerges from a 500 μm diameter source aperture and crosses the bichromatic standing wave beams, where it expands by $\approx \Delta v_B \times t_c = (\delta/16\omega_r)\lambda \approx 5\lambda$ for our parameters. Thus the bichromatic force does not cause very much spatial spreading. The atomic beam exits the light field and then expands freely in the cooled transverse dimension during a 63 cm flight to the detector. Measurement of the spatial distribution downstream is readily converted to the transverse velocity distribution.

The He atoms are detected using a microchannel plate and phosphor screen to image their transverse spatial distribution. The metastable 2^3S He atoms deposit their 20 eV internal energy when they strike one of the channels of the MCP, and the resulting amplified electron shower makes a visible bright spot on the fluorescent screen. The screen is viewed by a video camera whose frames are stored at 30 Hz. The transverse spatial spread at the end of the 63 cm flight is very much larger than our 24 mm detector. Thus, without any optical interaction the detector sees a flat He distribution, but spatial variations in detector sensitivity produce a nonuniform camera image and such images are used to correct the data images.

5. RESULTS

A. Spatial Phase Dependence of the Bichromatic Force

The spatial phase offset of the bichromatic standing waves where they are crossed by the atomic beam can be changed by varying the relative path length of the two bichromatic traveling waves used to form them. Observations of the force on the atoms demonstrates the dependence of the force direction on this spatial phase.

Initial measurements were taken with the path length difference between the two arms varied from $\pi c/4\delta$ to $\pi c/\delta$, where a spatial phase offset of $\lambda/2$ is produced by a path length difference of $\pi c/\delta$ (see Section 2.B.1). For each different path length, the light beams were collimated to produce approximately the same intensity profile at the mechanical slits that were imaged onto the atomic beam.

Figure 8 shows the response of the atoms to two values of the spatial phase offset, approximately $\pm\lambda/8$. Models of the bichromatic force predict a reversal of the direction of the force with this shift and it is demonstrated here, in agreement with the results of our simulations and the dressed atom model.

B. Cooling

A special data acquisition process was devised to optimize the experiment with respect to the different coupling coefficients depicted in Fig. 7(b). Since there is no single value of Ω that is correct for all three transitions, we took data over a range of values. The data were collected from video images of the transverse atomic spatial distribution at the detector as the laser power was varied over a large range by using an adjustable neutral density filter at the output of the transport fiber. Each video frame of the phosphor screen at a given laser power was averaged vertically for smoothing (the force is horizontal), and then we made a three-dimensional composite plot of these averages for the various Rabi frequencies, as shown in Fig. 9. We have a few dozen of these composite plots that take 2–3 min to record.

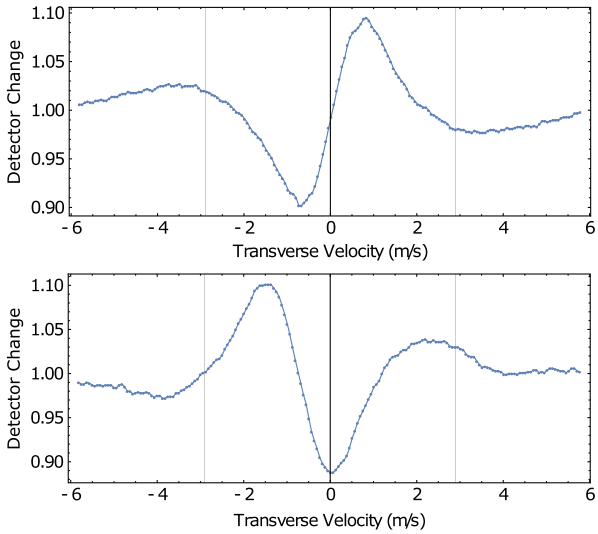

Fig. 8. The directionality of the bichromatic force is reversed with spatial phase offsets of $\sim \pm\lambda/8$ between the standing waves. These measurements were taken with interaction times of 380 ns. The velocity range of the force for these measurements was limited by insufficient Rabi frequency caused by the larger optical beam sizes used; however, the directionality is clearly demonstrated.

Figure 9(a) shows minimal redistribution of the atoms in the velocity range of the bichromatic force at low intensity, but clear evidence of redistribution when the laser power is increased. In this figure the darker purple represents a lower flux of He atoms and lighter areas indicate a higher flux.

A single velocity profile in the region of $\Omega = 2\pi \times 36$ MHz is plotted in Fig. 9(b). It shows that atoms starting in the velocity range from −6 to +2 m/s are accelerated into the range from +2 to +11 m/s without significant removal of those already there, and this is near the velocity limit of the force. Such a velocity change of ~9 m/s corresponds to ≈35 times the recoil velocity $\hbar k/M \approx 0.26$ m/s and is nearly the same as $\delta/k = 2\Delta v_B$. Note the good consistency between the measurements shown in Fig. 9 and the simulation in Fig. 4. We emphasize that this is accomplished in an interaction time of only $(5/6)t_{SE}$, and note that this confirms that the observed forces derive almost purely from stimulated effects, i.e., the bichromatic force without SE.

C. Experimental Issues

There are three separate effects that degrade the appearance of our cooled velocity distribution: the longitudinal velocity distribution of the atomic beam, the background of the atomic beam detection, and the ground state structure of the atoms.

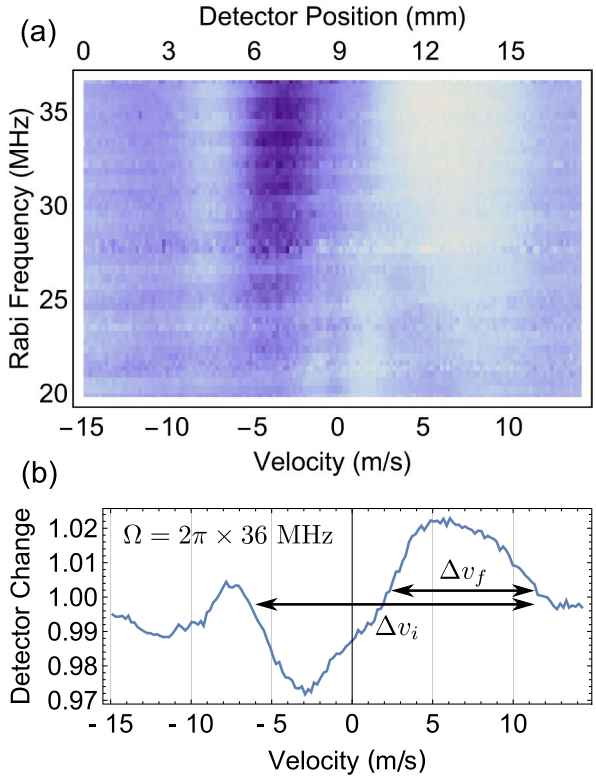

Fig. 9. Measured atomic spatial distribution taken with an optical slit width ≈230 μm corresponding to interaction time of 220 ns $< t_{SE}$ for longitudinal velocity ≈1050 m/s. The detuning was $\delta = 2\pi \times 25$ MHz corresponding to $\Delta v_B \approx 4.9$ m/s. In part (a) the dark regions represent reduced atomic intensity and the lighter regions increased intensity. The image has been corrected for detector inhomogeneity as discussed in the text. Part (b) shows a profile taken near the top of part (a) at $\Omega \approx 2\pi \times 36$ MHz. The initial (Δv_i) and final velocity widths (Δv_f) are indicated (figure from Ref. [2]).

1. Longitudinal Velocity Distribution

The longitudinal velocity distribution of our atomic beam spans about half the 1050 m/s center velocity [2]. The transverse velocity assignments shown in our data are for atoms traveling at the center velocity, and atoms with faster/slower longitudinal velocities will be deflected to smaller/larger positions on the detector, even for the same transverse velocity. This spatial spreading arising from the longitudinal velocity distribution causes our measurement of transverse velocity distribution widths to provide upper limits of the width of the true distributions.

We implemented a longitudinal time-of-flight detection technique to address this effect with limited success. Both the laser beams and the atomic beam detector were gated with a variable delay time between them so that the measurement could be sensitive to atoms within a selectable longitudinal velocity range. The optical beams were gated at 180 Hz by a mechanical chopper producing an "on" time of ∼200 μs, 10^3 times longer than the atomic interaction time, so that there were minimal switching effects. The atoms arrived at the detector at times determined by their longitudinal velocities. The high voltage for the microchannel plate was triggered by detection of the light pulse and was on for 240 μs after a set delay time. Since the flight path is 63 cm, a 600 μs delay between the gate centers corresponds to an average longitudinal velocity of 1050 m/s, and atoms with longitudinal velocities outside the bounds allowed by the finite width of the gates are not detected.

Our equipment limited us to those parameters that excluded only atoms in the wings of the longitudinal velocity distribution. This resulted in a large reduction of signal-to-noise ratio (S/N) based on the duty cycle of the detection (a few percent) and produced no significant effect on the cooled transverse velocity distribution. Better timing could improve this somewhat, but the repetition rate is always limited by the time necessary to prevent overlap of the cooled atomic pulses. This, along with the significant reduction of S/N required for further narrowing, discouraged additional measurements.

2. Detector Background

Second, our detector is sensitive to vacuum-ultraviolet light and other background emitted from the He discharge source so that there is only a 5%–10% peak-to-peak range of the profiles in Figs. 8 and 9(b). We verified that this represents nearly all the 2^3S He atoms by separately using a high-intensity ($s_0 \approx 1000$) laser tuned to the $2^3\mathrm{S} \rightarrow 2^3\mathrm{P}$ transition ($\lambda = 1.08$ μm) to remove all the atoms from a region on the detector, and measured the relative change in screen intensity.

3. Ground State Structure

Also, as discussed above, the Rabi frequencies of the applied standing waves for two of the three transitions shown in Fig. 7(b) are lower by about 13%. This means that over the range of laser intensities used for our measurements, there is no point where atoms in all three ground state sublevels experience the ideal Rabi frequency to achieve exact level crossings. As discussed in Ref. [14], even without such exact level crossings, there can still be a large force. For a truly two-level atom, this could be optimized, providing clearer results.

6. SUMMARY AND CONCLUSIONS

We have demonstrated the controversial notion of laser cooling in the absence of SE. Our results show a compression of the velocity distribution of a sample of atoms with minimal expansion of the sample size. At the end of the short interaction time with the bichromatic light field, the sample has not been able to expand by more than a few micrometers, although its initial size is hundreds of micrometers, and even this size is simply an apparatus limitation.

We use two frequencies tuned to either side of atomic resonance to implement the bichromatic force. Our premise is that the presence of multiple frequencies makes a dramatic change in the description of the laser cooling process, and we have exploited the two-frequency case to demonstrate this. We argue that the multilevel structure of real atoms has made enormous differences in understanding the laser cooling process, but the multifrequency case, even for a two-level system, is largely unexplored.

The width of our final velocity distribution has been reduced by ×2 in the region of interest, thereby reducing the temperature by ×4. Therefore, it is a compression of occupied

phase space volume because the spatial expansion of the atomic sample is ∼1%. We described how the longitudinal velocity distribution compromises the appearance of our data and limits our velocity space compression measurement to ×2, although it could actually be significantly more than we can measure.

Because the light field and the atoms must be considered as parts of the complete system under study, this process does not violate the dissipation requirements of Ref. [33]. The dissipation occurs when the light beams leave the system and are absorbed by the environment [1] (the system is open, not closed). Thus there is indeed the required dissipation.

In conclusion, both our measurements and our simulations demonstrate cooling and phase space compression of an atomic sample without SE using a two-frequency laser field. It works by restricting the atom–light interaction to a time short compared to a cycle of absorption followed by natural decay so that SE effects are minimized. The experiment uses an atomic transition with a relatively long excited state lifetime and a relatively short cooling time that makes this possible. This bichromatic force is the simplest extension from single-frequency forces, although there have been studies of other forces from polychromatic fields [17,30]. The potential for these polychromatic forces to cool should allow the extension of laser cooling to systems without closed cycling transitions, such as molecules [34], and in applications where space or access may be limited, such as short-distance beam collimation [35].

ONR (60256-1-1100814), U. S. Department of Education (GAANN).

We thank Martin G. Cohen for careful reading of the manuscript.

REFERENCES AND NOTES

1. H. Metcalf, "Entropy exchange in laser cooling," Phys. Rev. A **77**, R061401 (2008).
2. C. Corder, B. Arnold, and H. Metcalf, "Laser cooling without spontaneous emission," Phys. Rev. Lett. **114**, 043002 (2015).
3. R. Frisch, "Experimenteller Nachweis des einsteinschen Strahlungsrückstosses," Zeit. Phys. **86**, 42–48 (1933).
4. P. Meystre and S. Stenholm, eds., special issue on "The Mechanical Effects of Light," J. Opt. Soc. Am. B **2**, 1706–1861 (1985).
5. S. Chu and C. Wieman, eds., special issue on "Laser Cooling and Trapping of Atoms," J. Opt. Soc. Am. B **6**, 1961–2154 (1989).
6. W. Phillips and H. Metcalf, "Laser deceleration of an atomic beam," Phys. Rev. Lett. **48**, 596–599 (1982).
7. J. Prodan, W. Phillips, and H. Metcalf, "Laser production of a very slow monoenergetic atomic beam," Phys. Rev. Lett. **49**, 1149–1153 (1982).
8. J. Dalibard and C. Cohen-Tannoudji, "Dressed atom approach to atomic motion in laser light: the dipole force revisited," J. Opt. Soc. Am. B **2**, 1707–1720 (1985).
9. H. Metcalf and P. van der Straten, *Laser Cooling and Trapping* (Springer Verlag, 1999).
10. P. Lett, R. Watts, C. Westbrook, W. Philips, P. Gould, and H. Metcalf, "Observation of atoms laser cooled below the Doppler limit," Phys. Rev. Lett. **61**, 169–172 (1988).
11. J. Dalibard and C. Cohen-Tannoudji, "Laser cooling below the Doppler limit by polarization gradients—simple theoretical-models," J. Opt. Soc. Am. B **6**, 2023–2045 (1989).
12. J. Söding, R. Grimm, Y. Ovchinnikov, P. Bouyer, and C. Salomon, "Short-distance atomic-beam deceleration with a stimulated light force," Phys. Rev. Lett. **78**, 1420–1423 (1997).
13. M. Cashen and H. Metcalf, "Bichromatic force on helium," Phys. Rev. A **63**, 025406 (2001).
14. L. Yatsenko and H. Metcalf, "A dressed atom description of the bichromatic force," Phys. Rev. A **70**, 063402 (2004).
15. T. Lu, X. Miao, and H. Metcalf, "The Bloch theorem on the Bloch sphere," Phys. Rev. A **71**, R061405 (2005).
16. X. Miao, E. Wertz, M. G. Cohen, and H. Metcalf, "Strong optical forces from adiabatic rapid passage," Phys. Rev. A **75**, 011402 (2007).
17. D. Stack, J. Elgin, P. M. Anisimov, and H. Metcalf, "Numerical studies of optical forces from adiabatic rapid passage," Phys. Rev. A **84**, 013420 (2011).
18. A. P. Kazantsev and I. Krasnov, "Rectification effect of a radiation force," J. Opt. Soc. Am. B **B6**, 2140–2148 (1989).
19. V. Voitsekhovich, M. Danileiko, A. Negriiko, V. Romanenko, and L. Yatsenko, "Light pressure on atoms in counterpropagating amplitude-modulated waves," Zh. Tekh. Fiz. **58**, 1174–1176 (1988) [Sov. Phys. Tech. Phys. **33**, 690–691 (1988)].
20. R. Grimm, Y. Ovchinnikov, A. Sidorov, and V. Letokhov, "Observation of a strong rectified dipole force in a bichromatic standing light-wave," Phys. Rev. Lett. **65**, 1415–1418 (1990).
21. V. Voitsekhovich, M. Danileiko, A. Negriiko, V. Romanenko, and L. Yatsenko, "Observation of a stimulated radiation pressure of amplitude-modulated light on atoms," Pisma Zhur. Teor. Eksp. Fiz. **49**, 138–140 (1989) [JETP Lett. **49**, 161–164 (1989)].
22. R. Gupta, C. Xie, S. Padua, H. Batelaan, and H. Metcalf, "Bichromatic laser cooling in a 3-level system," Phys. Rev. Lett. **71**, 3087–3090 (1993).
23. T. Grove, B. Duncan, V. Sanchezvillicana, and P. Gould, "Observation of 3-level rectified dipole forces acting on trapped atoms," Phys. Rev. A **51**, R4325–R4328 (1995).
24. M. Williams, F. Chi, M. Cashen, and H. Metcalf, "Measurement of the bichromatic optical force on Rb atoms," Phys. Rev. A **60**, R1763–R1766 (1999).
25. M. Williams, F. Chi, M. Cashen, and H. Metcalf, "Bichromatic force measurements using atomic beam deflections," Phys. Rev. A **61**, 023408 (2000).
26. M. Cashen and H. Metcalf, "Optical forces on atoms in non-monochromatic light," J. Opt. Soc. Am. B **20**, 915–924 (2003).
27. R. Grimm, J. Söding, and Y. Ovchinnikov, "Coherent beam splitter for atoms based on a bichromatic standing light-wave," Opt. Lett. **19**, 658–660 (1994).
28. The value of $\Delta v_B \sim \delta/4k$ of Ref. [14] was found for different conditions.
29. J. R. Rubbmark, M. M. Kash, M. G. Littman, and D. Kleppner, "Dynamical effects at avoided level crossings: a study of the Landau-Zener effect using Rydberg atoms," Phys. Rev. A **23**, 3107–3117 (1981).
30. S. E. Galica, L. Aldridge, and E. E. Eyler, "Four-color stimulated optical forces for atomic and molecular slowing," Phys. Rev. A **88**, 043418 (2013).
31. J. Kawanaka, M. Hagiuda, K. Shimizu, F. Shimizu, and H. Takuma, "Generation of an intense low-velocity metastable-neon atomic-beam," App. Phys. B **56**, 21–24 (1993).
32. H. Mastwijk, "Cold collisions of metastable helium atoms," Ph.D. thesis (Utrecht University, 1997).
33. W. Ketterle and D. E. Pritchard, "Atom cooling by time-dependent potentials," Phys. Rev. A **46**, 4051–4054 (1992).
34. M. Chieda and E. Eyler, "Prospects for rapid deceleration of small molecules by optical bichromatic forces," Phys. Rev. A **84**, 063401 (2011).
35. M. Partlow, X. Miao, J. Bochmann, M. Cashen, and H. Metcalf, "Bichromatic slowing and collimation to make an intense helium beam," Phys. Rev. Lett. **93**, 213004 (2004).